In-situ measurements of magmatic volatile elements, F, S, and Cl, by electron microprobe, secondary ion mass spectrometry, and heavy ion elastic recoil detection analysis

Estelle F. Rose-Koga, Kenneth T. Koga, Jean-Luc Devidal, Nobumichi Shimizu, Marion Le Voyer, Célia Dalou, Max Döbeli

High precision *in-situ* measurements of volatile F, S and Cl by electron microprobe, secondary ion mass spectrometry, and elastic recoil detection analysis: a comparative study with application to melt inclusions

Estelle F. Rose-Koga[1], Kenneth T. Koga[1], Jean-Luc Devidal[1], Nobumichi Shimizu[2], Marion Le Voyer[3], Celia Dalou[4], Max Döbeli[5].

(1) Université Clermont Auvergne, CNRS UMR6524, IRD, OPGC, Laboratoire Magmas et Volcans, F-63000 Clermont-Ferrand, France

(2) Woods Hole Oceanographic Institution, Dpt Geology & Geophysics, MA, USA

(3) Smithsonian Institution, National Museum of Natural History, PO Box 37012, MRC 119, Washington, DC 20013, USA

(4) Centre de Recherches Pétrographiques et Géochimiques, UMR7358, CNRS - Université de Lorraine, BP20, 54501 Vandoeuvre-lès-Nancy Cedex, France

(5) Laboratory for Ion Beam Physics, ETH Zürich, Zürich, Switzerland

Abstract

Electron probe and ion probe are the two most used instrument for *in situ* analysis of halogens in geological materials. The comparison of these two methods on widely distributed glass standards (ex: MPI-DING) is needed. We report analyses of F, S and Cl concentrations in 3 geological glass samples (EPMA) and 10 referenced standards (EPMA and SIMS). F and Cl absolute abundances have been determined independently for three of the standards (ML3B-G, ATHO-G and KE12), via elastic recoil detection analysis (ERDA), to certify the accuracy of the cross-calibration EPMA-SIMS. The detection limits for EPMA are a 150 µg.g-1 for F, 20 µg.g-1 for S and Cl and for SIMS < 48 µg.g-1 for F, < 3 µg.g-1 for S and <19 µg.g-1. On SiO2-rich glass-standards, F and Cl measurements by ERDA highlight a matrix effect

during SIMS analysis of F and Cl. With the ERDA independantly measured value, we therefore propose an alternative calibration function to correct this matrix effect on the SIMS measurements of F, S and Cl. The application of F and Cl measurements on arc melt inclusions shows that over a wide range of H2O degassing, F/Cl remains constant for a given series of inclusions from a single volcano, suggesting F/Cl ratios are unchanged during volcanic degassing.

Keywords: F, Cl, SIMS, EPMA, ERDA, melt inclusion

Introduction

The behavior of trace volatile elements (magmatic volatile components other than H2O and CO2) in magmas has inspired many scientific contributions in the past decades (e.g. Baker et al., 2005; Wallace, 2005; Behrens and Gaillard, 2006; Fischer, 2008; Aiuppa et al., 2009 and reference therein). For an extensive review of the interest of halogens in Earth Sciences see Hanley and Koga, 2018 (in special volume by Harlov and Aranovich, 2018 and reference therein). In short, the interests go from partition coefficients of F, Cl and S between minerals and melt or fluid (e.g. Dalou et al., 2012; Zajacz et al., 2012; Bernini et al., 2012; Wu and Koga, 2013; Van den Bleeken & Koga, 2015; Kusebauch et al., 2015; Joachim et al., 2017; Iveson et al., 2018), to tackling mantle source compositions of these elements using melt inclusions (e.g. Straub et al., 2003; Bouvier et al., 2010; Le Voyer et al., 2010; Helo et al., 2012; Rose-Koga et al., 2012, 2014, 2017; Métrich et al., 2014; Cabral et al., 2014; Hartley et al., 2014; Jackson et al., 2015a) or using glasses (e.g. Kendrick et al., 2012; 2014a,b; 2015; Jackson et al., 2015b) or minerals (olivine: Broadley et al., 2019), to measuring the diffusion rate of volatile elements to assess magma ascent rates (e.g.

53 Llyod et al., 2014; Ferguson et al., 2016; Ruth et al., 2018) and assessing magma
54 degassing (e.g. Bureau et al., 2000; Edmonds et al., 2001; Balcone-Boissard et al.,
55 2010).
56 Bulk method for determining F and Cl contents in geological samples have improved
57 through the years and pyrohydrolysis followed by ion chromatography have improved
58 to reach detection limits of 0.2µg.g-1 (Michel and Villemant, 2003) even 0.1µg.g-1
59 (Blacone-Boissard et al., 2009), which remains a factor of 10 to 30 better than that
60 reported later with the same analytical tehnic by Marks et al. (2016; 10-20µg.g-1 for F
61 and 20-30µg.g-1 for Cl). Here we want to compare in-situ analytical technics for F
62 and Cl measurements because the study of smaller and smaller geological samples are
63 requiring intercalibration and comparison of the technics to make an educated
64 decision on which one to use to achieve the goal we have.
65 With recent advances of micro analytical techniques and melt inclusion studies, there
66 is a growing body of concentration measurements of relatively volatile, light-atomic-
67 mass elements (H, B, C, F, S, Cl) in MORB glasses and primitive melts of subduction
68 zone magmas (*e.g.* Sisson and Layne 1993; Métrich *et al.* 1999; Hauri et al., 2002;
69 Wade *et al.* 2006; Le Voyer *et al.* 2008, 2010; Bouvier et al., 2008; Rose-Koga *et al.*
70 2012; see also references in Wallace 2005). Other volatile element, moderatly heavier,
71 such as Br have also been successfully measured by secondary ion mass spectrometry
72 (Cadoux et al., 2017). While C and H and to a lesser extend S are likely to suffer
73 degassing (Dixon *et al.* 1995), halogens such as F and Cl (and probably Br) are often
74 under-saturated in these primitive basaltic melts, indicating that they did not
75 experience any degassing or fractionation event (*e.g.* Carroll and Webster 1994;
76 Bucholz et al., 2013).
77 Among the difficulties contributing to the limited comparison of the preexisting data,

was, suprisingly, the lack of published comparison of S, Cl and F measurements of standards between the two most used *in situ* analytical procedures: electron microprobe (EPMA) and the ion probe (SIMS). Recently, a F, S and Cl comparison between literature data obtain by EPMA and by SIMS (Le Voyer et al., 2019) concluded that inter-laboratory comparisons agreed within 10% for F and to a variable degree for S and Cl, and propose a quality controlled published-data summary table (Table S2 available through the EarthChem Library, http://dx.doi.org/10.1594/IEDA/111195).

Electron microprobes perform microanalysis of volatile elements, but the high detection limits of this technique (tens to hundreds of ppm) place limitations on many volatile studies (cf. Devine *et al.* 1995 and references therein). After a study improving the F measurement by EPMA (Zhang et al., 2016), the inter-calibration of EPMA and SIMS is timely and echoes conference abstracts about this recurrent subject (e.g. Rose-Koga et al., 2008; Guggino and Hervig, 2010). This will be the basis to push further the investigations for example of the degassing processes via experimental approach and *in situ* melt inclusion studies. Also it is noted that F, S, and Cl are among elements that LA-ICPMS can not measure (for measurements of major elements in melt inclusions by LA-ICPMS and intercalibration with EPMA and SIMS, see Pettke *et al.* 2004) and therefore their *in-situ* measurements in small objects such as melt inclusions rely solely on the development of their measurements by EPMA and SIMS, and their intercalibration.

Volatile-rich magmas are generally those of subduction zones. The current consensus is that arc magmatism is triggered by a flux, of either a volatile-rich fluid, or a silicate melt, derived from the subducting lithosphere (*e.g.* Gill 1981; Tatsumi and Eggins 1995), or a fluid somewhere between the two and termed supercritical fluid (Shen and

Keppler 1997; Bureau and Keppler 1999; Stalder *et al*. 2000). A large number of observations on isotopic compositions of arc lavas attest the necessity of slab flux in the constitution of lavas (e.g. Tatsumi and Eggins, 1995; Hanyu et al., 2012; Narvaez et al., 2018). Therefore, the nature of this flux and its interaction with solid mantle or with the subducting slab determines the element fractionation processes characteristic of this geodynamic setting (e.g. for Iwate volcano, Japan; Rose-Koga et al., 2014).

In this paper we measure F, S and, Cl by SIMS on a set of 6 glasses from the WHOI standard-set (ALV519-4-1, ALV1654-3, ALV1649-3, GL03-D51-3, GL07-D52-5, EN113-46D-2) to create 3 working curves. We use our 3 SIMS working curves to compare our SIMS measured values of 8 MPI DING glasses (ML3B-G, KL2-G, StHs6/80-G, GOR128-G, GOR132-G, ATHO-G, T1-G, KE12) and of 2 basaltic standards (VG2 and VG-A99) with our EPMA values. We also report independent absolute F and Cl values from elastic recoil detection analysis (ERDA) of three MPI DING glasses (KE12, ATHO-G and KL2G) which independently anchors our calibration curves. Finally, we give an example of application for EPMA and SIMS measurements of Cl and F in melt inclusions.

Standards and glass samples

All glasses and standards used have already been well documented elsewhere, and we summarize here the essential points. The set of 6 basalt samples used in this study for the SIMS analysis come from several sources (Table 1). The ALV standards are fresh basaltic glasses sampled during Alvin dives over the Famous area (ALV519-4-1: Shimizu 1998; Michael and Cornell 1998), and over the Galapagos Spreading Center 85ºW (ALV1654-3 and ALV1649-3; Embley *et al.* 1988; Perfit *et al.* 1998). GL standards are fresh basalt glasses from the Salas y Gomez seamount

area (GL03-D51-3 and GL07-D52-5; Simons *et al.* 2002). EN113-46D-2 is a fresh basaltic glass from the Endeavor spreading center (Simons *et al.* 2002).

For the other glass samples and standards we used six basalts (KL2-G, from Kilauea volcano, Hawaii; ML3B-G from Mauna Loa Volcano, Hawaii; VG2, *aka* USNM 111240/52, from the Juan de Fuca Ridge (Jarosewich 2002); VG-A99, aka A99, USNM 113498/1, from Kilauea volcano, Hawaii (Jarosewich *et al.* 1979); Alvin 2746-15, from 9-10ºN East Pacific Rise (Bowles *et al.* 2006); Alvin 2390-5, from the Siqueiros Transform, (Sims *et al.* 2002)), one andesite, (StHs6/80-G, Mt. St. Helens, USA, Jochum *et al.* 2000), two komatiites, (GOR128-G and GOR132-G both from Gorgona Island, Jochum *et al.* 2000), a rhyolite, (ATHO-G, from Iceland, Jochum *et al.* 2000), a quartz-diorite, (T1-G, from the Italian Alps, Jochum *et al.* 2000), two obsidians, (Sletta, from Iceland, courtesy from O. Sigmarsson; and KE12 from Eburru, Kenya; personnal communication of Malik and Bungard 1974 cited in Devine *et al.* 1984).

Analytical procedures

EPMA analysis

Electron microprobe analyses were performed with a Cameca SX 100 equipped with four wavelength dispersive spectrometers (WDS) at the Laboratoire Magmas et Volcans (Clermont-Ferrand). Major elements and volatiles were analyzed in separate analytical sessions with the following detailed conditions. Major elements in glasses were analyzed at an accelerating voltage of 15 kV, an 8 nA beam current and a 20µm defocused beam. These analytical conditions are well suited for glasses analyses; no geochemical instability (sodium loss principally) is detected even for silica rich samples (e.g. Oladottir *et al.* 2011).

Chlorine, sulfur and fluorine analyses were performed at 80 nA and with a 5 to 20µm defocused beam together with the trace element acquisition program proposed in the Cameca Peak Sight software. This quantification model takes into account the matrix composition of the glass to calculate the traces element concentration. ZAF data reduction was carried out by the means of the X-PHI model. The analytical standards were: natural scapolite for the Cl$K\alpha$ line, fluorite for F$K\alpha$ and VG-2 glass for S$K\alpha$. Sulfur concentration in VG-2 glass is 1340 µg.g-1 ; this value corresponds to the average of a compilation of published data (Dixon *et al.* 1991; Thordarsson *et al.* 1996; Thornber *et al.* 2002).

Sulfur and chlorine

Because sulfur speciation (S^{6+} or S^{2-}) induces changes in the S$K\alpha$ spectral position (Carroll and Rutherford 1988), prior to sulfur concentration measurement and for every sample, the S$K\alpha$ peak maximum was first located by using the regular automatic routine of the Cameca SX 100 software. Then, if the measured peak position differs from the one of the standard, the new value is changed in the analysis setup.

The selection of the diffraction crystals is driven by the achievements of the highest peak counts to reach very low detection limits and by looking at the region of the spectrum with no interfering peaks. Thus, chlorine and sulfur were analyzed successively by using a Large pentaerythritol (LPET) crystal.

Fluorine

The case of fluorine is more complex. This element can be measured either with a W/Si multilayer crystal (PC1) or with a thallium acid phthalate crystal (TAP).

Multilayer crystal allows high precision and accuracy measurements together with low detection limits. Unfortunately, for iron-bearing minerals or glasses, the F$K\alpha$ peak is strongly overlapped by the shoulder of a strong Fe$L\alpha$ line. Different studies (Todd 1996 ; Witter and Kuehner 2004) have proposed an electron microprobe method for analyzing F in Fe-bearing minerals and glasses using multilayer crystals that overcomes the spectral interference. This method is based on the linear relationship existing between the iron concentration of fluorine-free minerals (olivine and pyroxenes essentially) and the number of counts at the F$K\alpha$ peak position in the same fluorine-free minerals. Thus, the Fe$L\alpha$ contribution (i.e. the background) can be easily deduced and quantified from the total iron concentration of the sample and subtracted from the bulk F*Ka* peak counts. However, the calibration curve of this model is only found for the analysis of Fe^{2+}-bearing minerals. In transition metals of the first row, the L-spectra exhibit peak position shifts as a function of the oxidation state (Fialin *et al.* 2001, 2004). The omission of the self-absorption induced shift of the $L\alpha$ peak between Fe^{2+} and Fe^{3+} could lead to the overestimation of the background counts at F*Ka* peak position and thus to an underestimation of the fluorine content. The correction method established by Witter and Kuehner (2004) should be only applied for pure Fe^{2+}-bearing minerals and glasses. In order to overcome this problem, we analyzed fluorine using TAP diffraction crystals although the detector is significantly less efficient than PC1. To improve its counting statistics (precision and detection limit), fluorine was measured simultaneously on 3 spectrometers according to the Cameca multi-spectrometers counting routine. On top of the choice of the detector, we tested CaF_2 and Durango apatite standards for F calibration, and concluded that CaF_2 provides generally consistent results, most likely due to known F X-ray excitation issue of apatatite (Stromer et al., 1993).

The challenge with traces elements analysis in glass is to find a compromise between low detection limit, i.e. the used of high beam current, long counting time, and limited beam damages. Volatile loss during the analysis is minimized through the used of a protocol derived from the CSIRO-trace routine (Robinson and Graham 1992). The total counting time (peak and background) for a single analysis is 40 sec and is divided as follow: 10 sec on peak and background for chlorine and sulfur but 60 sec on peak and background for fluorine (20 sec per spectrometer). Low detection limit is achieved by increasing the number of analysis on the same point, thus by improving the singal-to-noise ratio. After each analysis, the beam is shielded for 20 sec allowing the sample to cool down. Total volatiles concentration is calculated from the sum of the counts from the successive iterations. With 15 kV accelerating voltage and 80 nA beam current, for a total Cl and S peak counting time of 100 sec and 600 sec for F. Typical detection limits for F, Cl, and S were 150, 50 and 50 $\mu g.g^{-1}$, respectively.

SIMS analysis

Sample preparation for SIMS

The standards are mounted in high purified indium metal (e.g. Hauri *et al.* 2002; Le Voyer *et al.* 2008) in a 1 inch diameter aluminum ring, put in ultrasound in pure ethanol then in distilled water for 10 minutes, respectively. Indium is used because epoxy can contain significant amounts of volatiles that can degass during the analysis and increase the background signal. The mount is dried carefully in an oven overnight. The mount is finally gold coated before analysis and kept overnight in high vacuum (low 10^{-8} torrs) until being inserted in the sample chamber.

228

229 ## Method

230 The measurements for the working curve calibrations were done on a set of 6
231 glass standards (Table 1), on the ion probe Cameca 1280 of Woods Hole
232 Oceanographic Institution (MA, USA). We used a Kohler illumination with a primary
233 beam current of 1.5 nA Cs^+ primary positive beam, and negatively charged secondary
234 ions were extracted through a nominal accelerating potential of 10 kV. Due to
235 implantation of Cs^+ ions and extraction of both negatively charged secondary ions and
236 electrons, positive charging of the sample surface must be compensated with the use
237 of an electron flood gun which delivers electrons to the sample surface. The isobaric
238 interference were filtered by an energy slit opening at 50 eV and the contrast aperture
239 at the cross over was large (400 µm). The entrance and exit slits are closed to achieve
240 a mass resolution of $M/\Delta M=5800$.

241 We presputtered the samples surface during 180 seconds while applying a
242 raster of 30×30 µm. The field aperture (of 8000) corresponds to an area of 15×15 µm,
243 is inserted into the image plane. This means that only the ions originating from the
244 central 15 µm of the flat-bottomed sputtered-crater are admitted into the mass
245 spectrometer. The elimination of stray ions sputtered from the crater walls and
246 desorbed from the sample surface results in very low volatile backgrounds (routinely
247 about 0.05–0.1 counts per second for the counting system at half mass positions with
248 the primary beam and the electron gun on). We counted 8 sec on ^{19}F, 5 sec on ^{30}Si, 5
249 sec on ^{32}S and 8 sec on ^{35}Cl. One analysis was composed of 2 blocks of 10 cycles and
250 took less than 15 min per spot. Intensities of ^{19}F, ^{32}S and ^{35}Cl were collected
251 cyclically by an electron multiplier, processed through pulse-counting electronics and
252 normalized to ^{30}Si for concentration calculations.

Calibration

Earlier studies that have involved Cs^+ beam were performed on small format SIMS (Cameca 6f, Hauri *et al.* 2002). But hydride interferences, such as SH^-, are difficult to effectively eliminate using the energy filtering technique (Shimizu *et al.* 1978) available on small format Cameca instruments (e.g., IMS 3f/4f/5f/6f). The high mass resolution of the SIMS 1280 of WHOI is required to eliminate the $^{34}S^{1}H$ interference on ^{35}Cl (MRP>5120) without giving up transmission significantly (Fig. 1c). The SIMS calibration curves for F, S and Cl are shown in Fig. 2. They are regressions of ion probe signals (x-axis) compared to known EPMA concentrations (y-axis). The former is the intensity ratio of two elements times the SiO2 concentrations of each standards, the numerator of the ratio being the element of interest and the denominator is a matrix element common to all samples (e.g. $^{19}F/^{30}Si$). Typically, here ^{19}F, ^{32}S and ^{37}Cl are normalized against ^{30}Si. This provides a robust analysis little influenced by primary beam fluctuations or by ionization efficiency changes owing to matrix effects (Shimizu and Hart, 1982). In fact, the calibrations for F, S and Cl are free of significant matrix effects. The calibration curve is determined at the beginning and at the end of each session to assure no significant drift has taken place.

Detection limit

With the calibration curves of the standards, one usually attributes the Y-intercept of the linear regression to the detection limit (*e.g.* Ihinger *et al.* 1994). This methods is not accurate enough and depends on the uncertainties of the regressed data, the leverage of the data for the higher concentrations being potentially

unreasonable. Ideally, only the measurements of standards with F, S, and Cl concentrations lower than the expected background can give the detection limit (see Koga et al., 2003, for this procedure during low hydrogen concentration measurements by SIMS). It was not a simple task to verify ppm-level abundance, and we adapted calibration without explicitly identifying zero point count rate (Table 1). Some studies have used adapted "blank" material such as San Carlos olivine and synthetic forsterite (Hauri et al. 2002, Le Voyer et al. 2017). With what was available to us we calculated detection limits 48 µg.g-1 for F, 3 µg.g-1 for S and 19 µg.g-1 for Cl (Fig. 2). These values are close to the zero intercept and considering the error on the y-intercept is as large as the value itself, the linear regression of the calibration curve is equivalent to forcing the regressin through zero. The slopes between forcing the linear regression through zero (red curve Fig. 2) and classic linear regression (blue curve Fig. 4) is identical within error. A detection limit of <1 µg.g-1 for F, S, and Cl was previously reported with a 6f ion probe (Hauri *et al.* 2002; <2 µg.g-1 for F; Guggino and Hervig 2010). With a 1280 ion probe detection limits down to 0.2 µg.g-1 for S and Cl, and 0.1 µg.g-1 for F can be achieved with blank standards (Le Voyer et al., 2019). Our analytical standard error (σ over the 20 cycles) was typically 0.6 % for F, S and Cl (1% Le Voyer et al., 2019) and the reproducibility on the standards (2RSD) was 6.3, 3.5 and 5.2%, respectively (n=14, ALV519-4-1; comparable to 5.8, 7.6 and 10.8%, respectively, on in-run standard glass P1326-2, Helo et al., 2011; 7, 4 and 7%, respectively on glass VG2, Le Voyer et al., 2019).

Elastic Recoil Detection Analysis (ERDA)

ERDA is an absolute measurement independent from the two previous methods (EPMA and SIMS). Absolute because it consists of a shock between the

nuclei of 2 atoms and the radii of the two nuclei (for example ^{19}F and ^{127}I) are known with great precision, and therefore the ERDA method do not require any standard to perform a measurement. ERDA has previously been used to measure hydrogen in geological materials (e.g. Mosbah et al., 1990; Bureau et al., 2009) or to intercalibrate with infrared spectroscopy measurements (e.g. Aubaud et al., 2009; Withers et al., 2012). The ERDA were made at ETH Zurich, in the Ion Beam Physics laboratory of the Paul Scherrer Institut. We used a primary ion beam of heavy ion ^{127}I at 12 MeV. This iodine beam was produced by EN-tandem accelerator via cesium (Cs) sputtering of AgI. For lower projectile energies Time of Flight-ERDA (ToF-ERDA) is a widely used technique. The analytical protocol is only briefly explained in the following, full details can be found in C. Kottler *et al.* 2006 (and reference therein). The beam hits the polished plane of the sample with a low angle and the scattered element of choice (F and Cl, here) are detected by the ToF-ERDA dectector at the fixed angle of 36º. The recoil masses are identified by means of a coincident measurement of the particle velocity and total energy. The recoil energy for ^{19}F is 3.5 MeV and that of ^{35}Cl is 5.3 MeV. Here a gas ionization chamber (GIC) instead of silicon detectors has been used for energy measurements because silicon detectors suffer from considerable radiation damages. This standard-free method gives absolute F and Cl concentrations. The shape of the beam on the sample is a rectangle of 1 mm × 4 mm but only a small part of it was actually targeting the sample, the rest was hitting the surrounding indium. A classical ERDA graph displays a time of flight curve for each ion versus energy (Kottler *et al.* 2006). These curves are processed to extract a spectrum for each elements (Fig. 3a, b, c)

Results

There is a good general agreement on mafic standards for the measurements of F, S and Cl between EPMA and SIMS above a certain treshold of concentrations, >150 µg.g-1 for F, and >20 µg.g-1 for S and >20 µg.g-1 for Cl (Fig. 4). For F<150 $\mu g.g^{-1}$ SIMS can measure differences in F concentrations with a precision better than 10% relative when EPMA has a precision equal to the measured value (Fig. 4a). The performance of both EPMA and SIMS are in excellent agreement for Cl measurements down to 20 µg.g-1 (Fig. 4c). But for S measurements, SIMS can measure S concentrations below 10 µg.g-1 when EPMA will not measure resolvable difference in standards with S<10 µg.g-1 (Fig. 4b).

The glass standards measured here have reported value that can vary up to a factor of 10 for certain elements (ex: Cl in StHs6/80; Table 2). Nonetheless, overall we note that technical improvement of in-situ instruments make it possible to reach interlaboratory agreements. Our EPMA and SIMS measurements most of the time agree within error with the reported values published since 2006 (ex: Jochum et al., 2006), simply improving the precision in some cases. When they do not agree, we can invoke millimeter scale heterogeneity of the standards. They have been reported for trace elements in the ATHO-G rhyolite (MPI-DING; Borisova et al., 2010) and cautious must apply when choosing your standards to perform micro-analysis. For example it is clear from Table 2 that the ATHO-G piece that we have is very different than the piece measured by SIMS in Jochum et al, 2006, and much closer to the composition of that of Oskarsson et al. (1982) and this has nothing to do with the quality of the analysis. In this respect, ATHO-G and StHs6/80-G appears to be heterogenous for F, S and Cl depending on the pieces you have. Also the 2σ error we report for our EPMA are 9 times out of 10 better than previously reported,

352 demonstrating that the proposed settings for halogen measurements by EPMA are
353 particularly well suited.
354 The ERDA results for F and Cl in ATHO-G, KE12 and KL2-G anchors independantly
355 the calibration curves for F and Cl. We note that the ERDA values for F and Cl of the
356 two SiO2-rich standards, are closer to the EPMA values than the SIMS values (Fig. 4a
357 and 4c), and the ERDA measurement on the basalt standard KL2-G was difficult to
358 assess because of the high detection limit of the ERDA.
359
360 **Discussions**
361 *Precision and accuracy*
362 The lowest concentrations we measured were samples GOR-128 and GOR-
363 132 for F and S and sample StHs for Cl (Table 2). While EPMA measurements tend
364 to level out around 10 µg.g-1 concentration for S (Fig. 4b), SIMS measurements are
365 precise to µg.g-1 level for S and Cl (Fig.4b and c). For F, S and Cl, SIMS
366 measurements always display smaller error bars (Fig. 4a, b, c). Samples with
367 concentration in S, Cl > 100 µg.g-1 are analyzed with similar precision with both
368 methods. Measurements of F remains up to 5 times more precise with SIMS than
369 EPMA on the basis of analytical precision based on counting statistics and for F
370 concentration above 100 µg.g-1. Because many standard values are still tied to EPMA
371 measured samples, it appears that the uncertainty of the slope and intercept (Fig. 2)
372 contributes to the final uncertainty similar to EPMA values (Table 2). Therefore, it is
373 strongly recommended to use SIMS when the interest of measurement is to detect
374 variations of concentration among similar samples with a high precision, while EPMA
375 can certainly provide a rapid, good assessment of trace volatile abundances above a
376 certain threshold.

Matrix effect

It is particularly notable that some measure values by SIMS (reported for ATHO-G and KE12; Table 2) significantly differ from those of EPMA and ERDA. Fig. 4 also shows that higher SiO2 glasses (e.g. ATHO and KE12) plot on the right side of the 1:1 line, outside of +/-20 % bound (a conservative external reproducibility range), indicating SIMS measurements are higher than EPMA and ERDA. While such offset is not present for mafic glasses which have similar SiO2 content as the calibration standards. This offset is present for measurements of F, S and Cl. This systematic disparity related to the composition of material analyzed is called matrix effect, in which the secondary ion emission is influenced by change either structual or compositional variation of the matrix.

The relative sensitivity factor (RSF) describes a bias of an elemental ratio introduced by SIMS: RSF = (Ci/Cref)×(Iref/Ii), where Ci and Cref are the known atomic concentration of mass i and mass ref, respectively and I denotes the measured signal intensity. Essentially, the slope of the calibration function is a representative RSF of several calibration standards. It should be noted that RSF cannot distinguish bias of the signal of interest (e.g. I_F, I_S, and I_{Cl}) from the signal of reference (I_{Si}). Fig. 5 shows the value of RSF calculated for the samples of Fig. 4 as a function of SiO_2, excluding the EPMA data below detection limit. It appears that RSF is slightly negatively correlated against SiO2, consistent with a presence of matrix effect for the high SiO2 samples. However, considering the scatter of RSF values, the appearent negative correlation has only slight statistical significance. The data aquired here is not sufficient to decern the exact role of the “matrix effect”. Because of such tendency, van den Bleeken and Koga (2015) concluded from a similar analysis that as a first

order, one should be able to approximate the abundance of these element without correction.

Choices of calibration method

Reference mass: concentration analysis by SIMS requires a ratio of the element of interest (F, S, Cl here) over an element that constitute the matrix. For silicate glasses, it is commonly Si is chosen (Shimizu and Hart). 30Si is commonly selected for its low abundance permitting the use of electron multiplier detector. However, depending on the SIMS facility, different reference mass is used. For example, 28Si detected with Faladay cup can be used as the reference mass, as well as 18O- or 16O-. In general, emission of negative oxygen atom is approximately 10 times better than Si but this does not seems to result in significantly more stable signal. While it will require further study to assess the advantages and disadvantages regarding the choices of the reference mass, a comparison results from different SIMS labs concluded that it would not influence the measurement significantly (in the electronic supplement, van den Bleeken and Koga, 2015).

Calibration curves: a linear function that converts a SIMS intensity ratio to a concentration can be expressed in following two ways.

$$[\text{F, S, Cl ppm}] = \text{Coef} \times (I(\text{F, S, Cl}) / I(\text{Si})) \times [\text{SiO2}] + \text{Intercept} \quad \text{(eq. 1)}$$

$$[\text{F, S, Cl ppm}] = \text{Coef} \times (I(\text{F, S, Cl}) / I(\text{Si})) + \text{Intercept} \quad \text{(eq. 2)}$$

where, brackets indicates concentration and I(x) indicates SIMS intensity (i.e. count rate) of mass x. Coef, and Intercept are constants determined by fitting the function using known concentration standards. Among SIMS measurements reported, these two equations were commonly used. The eq. 2 is sufficient for the measurement with a good match of sample and standard matrices (i.e. similar SiO2 content). In the

current study, we adapted eq. 1, which corrects for variable SiO2 content (e.g. 50% basalt and 70% rhyolite). However, it should be noted that the eq. 1 does not correct for the matrix effect.

Recognising the weak correlations between SiO2 and RSF, we have explored a potential modification of the working curve function in an aim to optimize the accommodation of SiO2 viriation in silcate glass. Taking Cl as an example, the eq. 1 can be rearranged to show the relationship with RSF.

$\{[Cl] - [Intercept]\}/\{[SiO_2]\} \times k = RSF \times (I_{Cl}/I_{Si})$ eq. (1')

Where k is a conversion factor for concentration ratio to atomic ratio, thus Coef = RDF/k. Inspecting Fig. 5, we decided to explore two functional forms relating RSF and SiO2.

$RSF = a / [SiO2] + b$ (eq. 3)

$RSF = c \times [SiO2] + d$ (eq. 4)

Substitutig eq. 3 or eq. 4 into equ. 1', the working calibration curve will be in following form.

$[Cl] = ak(I_{Cl}/I_{Si}) + bk(I_{Cl}/I_{Si})[SiO2] + Intercept$ (eq. 5)

$[Cl] = dk(I_{Cl}/I_{Si})[SiO2] + ck(I_{Cl}/I_{Si})[SiO2]^2 + Intercept$ (eq. 6)

Table 3 shows the result of regression with above equations. For the regression, in addition to six calibration standards, three high Si samples are added T1g, ATHO, and KE12. Inspecting the results of the regression, eq. 6 consistently produced better fit, although slight, than eq. 5. On top of this,'ck' term is significantly smaller than 'dk' term in eq. 6. This suggest that the role of additional term in correcting the matrix-dependent calibration is minor. This conclusion is again consistent with that of van den Bleeken and Koga (2015) in which authors concluded the use of eq. 1 is sufficient to determine trace halogen concentration in a wide range of silicate glasses. Lastly,

452 recalculated concentration using eq. 6 is presented in Table 2, indicated as SIMS [eq.
453 6].
454
455 **Applications to arc lava olivine-hosted melt inclusions**
456 Subduction zones have generally volatile-rich magmas. The magmas are produced by
457 mantle wedge melting induced by slab-derived fluids. Lava erupting from arc these
458 volcanoes are at least partially degassed. Olivine hosted-melt inclusions found in
459 these lavas, are silicate droplets trapped in a host-mineral (olivine here) are less
460 affected by degassing, and shielded from interaction with their surrounding in the
461 magma chamber and during magma ascent. Especially for the halogens Cl and F, at
462 pressure and temperature conditions of melt inclusion formation, they are less prone
463 (1) to degassing (if at all) than H_2O (e.g. Carroll and Webster, 1994; Métrich and
464 Wallace, 2008), (2) to diffusing through the host-olivine (e.g. Bucholz et al. 2013;
465 Lloyd et al. 2013; Le Voyer et al. 2014). Recent experimental results have
466 determined F and Cl partition coefficients between melt and crystals (Dalou et al.,
467 2014) and put forward that the large variation of F/Cl in arc melt inclusions resulted
468 from the composition, the amount of slab agent and the degree of melting.
469 Our recent melt inclusion data combined with litterature data show that although F/Cl
470 ratios in arc melt inclusions can vary between 0.1 and 4 (see fig 5A in Dalou et al.,
471 2014), within each sample suite, for each volcano, F/Cl is relatively constant, over a
472 range of H_2O abundance (Fig. 6). The F/Cl is normalized to the average F/Cl of each
473 arc, so that all constant F/Cl ratio gather around the unity value. This illustrates that
474 while H_2O can vary due to degassing prior to (or after) the entrapment of melt
475 inclusions, pre-entrapment F/Cl values remain constant. The same conclusion can be
476 drawn with F/Cl plotted against CO_2, F, or Cl. This systematics demonstrate either 1)

F and Cl remain in melt during degassing, a conclusion reached for example by Bucholz et al., (2013) or 2) partitioning of F and Cl between fluid and magma is identical (Wu and Koga, 2013; Dalou et al., 2014). While we focus on the incompatible behaviors of Cl and F in basaltic melt, it should be noted that there exists a number of studies and experimental work concerning Cl and F behavior in evolved magmas, with specific application to volcanology and ore deposit formations (e.g. Webster, 1990, 1992; Brenan, 1993; Giordano et al., 2004). Their results on halogen partitioning in fluid - evolved melt systems show that Cl and F are strongly partitioned into the fluid at crustal degassing conditions (Webster et al., 2018; Dolejs and Zajacz, 2018). But even if the halogens appear to degas during magmatic evolution in mid-to- shallow crust, Cl and F in primitive basalts, especially in melt inclusions, appear to retain the information of magma genesis (Koga *et al.* 2009; Bucholz et al., 2013; Rose-Koga et al., 2012, 2014) along with other lithophile trace elements (such as REE). The subduction input/output mass balance calculations show that nearly 100% of Cl coming in subduction is incorporated in arc magmatism, compared to only about 50% of F (e.g. Straub and Layne 2003; Wallace 2005). Therefore Cl and F are ideal tracers to identify the fractionation process between the slab and the flux originating from it, especially since they are scarcely present in the mantle (F reservoirs, see for example Koga and Rose-Koga, 2016; 2018). It is generally considered that Cl shows an affinity to volatile-rich fluid and F shows an affinity to silicate melt (e.g. Schilling *et al.* 1980). An experimental study on F fractionation between aqueous fluid and mineral at pressures and temperatures relevant to subduction zone settings, demonstrated for example the strong affinity of F for the silicate phase (Wu and Koga, 2013).

Studies of halogens in magmatic products cover a wide range of applications. Studies involving F and Cl measurements (and their ratios with trace elements) on arc samples are able to decipher the transport vector (melt and/or fluid) from slab to surface (e.g. Rose-Koga et al., 2014). Also F and Cl measurements combined with Pb isotopes can bring new constraints on the source of OIB lavas (e.g. Peterson et al., 2014) or on the volatile contents of the mantle endmembers (e.g. Rose-Koga et al., 2017). Halogens combined with Sr isotopes can decipher between mantle source Cl-enrichment and brine assimilation (e.g. Reinhardt et al., 2018)

Implications

F and Cl measurments by EPMA and SIMS have a general good agreement on standards glasses available to the scientific community (MPI-DING, Jochum et al., 2006). These are the two most common insturment for *in situ* halogen measurements and finally there performance are analysed and compared. The F and Cl ERDA measurements on 3 standards anchors independantly the EPMA-SIMS comparison curves and gives absolute F and Cl concentrations for these standards. The ERDA results also highlight the fact that there is a matrix effect on SIMS measurements of F and Cl in high-SiO2 standard. We propose a new equation to correct this matrix effect in the SIMS F and Cl data of high-SiO2 samples.

We can now use, indifferently EPMA or SIMS for F and Cl measurements, on a large SiO2 range covering most of the geological samples.

Conclusions

An intercalibration of F, Cl and S measurements between EPMA and SIMS is reported for 10 glass-standards. Both analytical methods are in excellent agreement

for standards with concentrations in these volatiles elements above 150 µg.g-1 for F and above 20 µg.g-1 for S and Cl. However, SIMS has a lower detection limit and is preferable in the case of low concentration samples. The ERDA measurements independently confirms and anchors our data. This study revealed a shift between acidic and mafic glass-standard on our ERDA data, thus requiring (1) cautious in the choice of standard materials, and (2) separate SIMS calibrations with standards covering the SiO_2 range of the samples. An alternative is to use the equation 6 that we propose to account for this matrix effect on the SIMS measurements of F, S and Cl. In arc melt inclusions, F/Cl ratios of series of inclusion from single volcanoes, remain constant over a large range of H2O concentration, suggesting these halogen do not degass. On a broader point of view, halogens such as F and Cl (also Br and I), associated with radiogenic isotopes and trace element ratios, are promising new tracers of fluid and/or melt transport from their source regions and for degassing processes.

Acknowledgement: EFR-K thank O. Sigmarsson for the Sletta sample. EFR-K and KTK acknowledge support from Region Auvergne Rhone Alpes (SCUSI program). This is Laboratory of Excellence *ClerVolc* contribution number xxx.

546 Figure caption

547

548 Fig. 1: Secondary ion spectra at nominal masses, 19 (a), 32 (b) and 35 (c) for a basalt
549 glass (ALV519-4-1) to illustrate the resolution of isobaric interferences at
550 M/ΔM=5800 (10% definition). This basalt glass contains 90 µg.g-1 F, 950 µg.g-1 S,
551 and 45 µg.g-1 Cl (Helo et al., 2011; Table 1).

552

553 Fig. 2: SIMS calibration curves for abundances of (a) fluorine, (b) chlorine, (c) sulfur
554 in basalt glasses. The lines correspond to different fit. The red line is a linear
555 regression line forced through zero, the blue line is a classic linear regression line, the
556 y-intercept giving the detection limit of the analyzed element. Since any of those fit
557 are satisfactory within the error bar, we consider the calibrations are linear over
558 several orders of magnitude in S, Cl, F concentrations.

559

560 Fig. 3: Elastic recoil detection analysis (ERDA) spectra for oxygene ^{16}O (a), fluorine
561 ^{19}F (b) and chloride ^{35}Cl (c). On the y-axis are reported the counts and on x-axis, the
562 mass. This is the example of the measurements done on the standard MPI-DING glass
563 KE12 (Jochum et al., 2006).

564

565 Fig. 4: concentrations of F (a), S (b) and Cl (c) measured by SIMS versus that
566 measured by EPMA (circles) and ERDA (square, when applies) in a log-log plot.
567 Standards are categorized according to their SiO2 contents into mafic, intermediate
568 and acidic.

569

570 Fig. 5: RSF (the relative sensitivity factor) is plotted against SiO2 concentration in
571 glass samples. RSF is determined for individual analysis of known samples. (a) RSF
572 of fluorine, (b) of sulfur, and (c) of chlorine are shown here. There exist a slight
573 negative slope for all the panels however due to scatter of measurements, the trend is
574 not statistically significant. There are less number of RSF values as many of sulfur
575 concentrations are below EPMA detection limit and there were no independent way to
576 verify their concentrations.
577
578 Fig. 6: F/Cl ratio normalized to the average versus H_2O concentrations in wt%.
579 Symbols are for olivine-hosted melt inclusions from different arcs (Sommata: Rose-
580 Koga et al., 2012; Ecuador: Le Voyer et al., 2008; Narvaez et al., 2018; Shasta: Le
581 Voyer et al., 2010; Mariana: Shaw et al., 2012; Lesser Antilles: Bouvier et al., 2008,
582 2010; Vanuatu: Sorbadère et al., 2011).
583

584 Tables

585 Table 1: F, S, Cl and SiO_2 measurements in 6 basalt glasses with the corresponding
586 analytical methods and references. They are the glass-standards used for the
587 calibration on the WHOI SIMS.

588 Table 2: Report of F, Cl, S and SiO_2 concentration measurements in 10 referenced
589 material (*) and 3 other basaltic glasses ($\pm$ is 2σ). Analytical methods and references
590 are specified.

591 Table 3: Result of error weighted regression of Eq. 5, and Eq. 6

592

593

594

595

596

597

598

599

600

601

Table 1: F, S, Cl and SiO_2 measurements in 6 basalt glasses with the corresponding analytical methods and references. They are the glass-standards used for the calibration on the WHOI SIMS.

	F [ppm]	±	S [ppm]	±	Cl [ppm]	±	SiO_2 wt%	Mehod; Reference
ALV519-4-1	90	30	950	95	45	23	48.9	EPMA; [1]
ALV1654-3	997	150	1562	78	2914	146	56.7	EPMA; [1], [2]
ALV1649-3	445	67	1640	82	1433	72	51.5	EPMA; [1], [2]
GL03-D51-3	299	45	1126	57	182	18	49.5	EPMA; [1], [3]
GL07-D52-5	431	65	1183	59	322	32	48.6	EPMA; [1]
EN113-46D-2	124	37	877	88	45	23	49.5	EPMA; [1], [3]

[1] Helo et al., 2012; [2] Michael & Cornell, 1998; [3] Simons et al. 2002.
Relative analytical error for F concentration >200 ppm is 15% and F<200 ppm is 30%.
Relative analytical error for S concentration > 1000 ppm is 5% , between 100 to 1000 ppm is 10% and < 100 ppm is 50%.
Relative analytical error for Cl concentration >400 ppm is 5%, between 50 and 400 ppm is 10%, and Cl< 50 ppm is 50%.
Errors of these standards are assessed on the long term reproducibility.
SiO2 was measured by EPMA

Table 2: Report of F, Cl, S and SiO_2 concentration measurements in 10 referenced material (*) and 3 other basaltic glasses (± is 2σ). Analytical methods and references are specified.

	F [ppm]	±	S [ppm]	±	Cl [ppm]	±	SiO_2 wt%	Method; Reference
ML3B-G*	70	18	1.2	0.12	7.5	1.4	51.4	SIMS; [1]
			100	100	110	33		EPMA; [1]
			30	30	60	18		EPMA; [1]
	64;57;69	30;20;30						EPMA; SIMS; PIGE; [2]
	71	14	5.2	0.1	36	1		SIMS; [WHOI this study]
	61	**11**	**5.1**	**0.2**	**32**	**2**		**SIMS; [eq. 6, this study]**
	48	*68*	*17*	*13*	**32**	**21**	**50.7**	**EPMA; [LMV this study]**
StHs6/80-G*	320	32	2.7	0.3	184	18	63.7	SIMS; [1]
			40	40	210	42		EPMA; [1]
					230	69		EPMA; [1]
	139;122;155	2;2;2						EPMA; SIMS; PIGE; [2]
	<d.l.		4.3	0.1	27	0.6		SIMS; [WHOI this study]
	<d.l.		**4.1**	**0.2**	**24**	**0.8**		**SIMS; [eq. 6, this study]**
	28	*35*	*19*	*1*	**21**	**11**		**EPMA; [LMV this study]**
T1-G*	321	32	2.6	0.3	113	14	58.6	SIMS; [1]
			30	30	100	50		EPMA; [1]
					130	65		EPMA; [1]
			0.92		119			LA-ICPMS; [3]
			1.94					LA-ICPMS; [3]
	107;94;119	6;6;8						EPMA, SIMS, PIGE; [2]
	274	39	6.0	0.2	175	8		SIMS; [WHOI this study]
	207	**29**	**5.7**	**0.2**	**135**	**14**		**SIMS; [eq. 6, this study]**
	154	47	*20*	*8*	**158**	**7**	**57.5**	**EPMA; [LMV this study]**
GOR128-G*	25	3	4.3	0.4	11.7	1	46.1	SIMS; [1]
			30	30	50	35		EPMA; [1]
					40	50		EPMA; [1]
	<d.l.		8.3	0.2	38	0.9		SIMS; [WHOI this study]
	<d.l.		**8.4**	**0.3**	**33**	**1.7**		**SIMS; [eq. 6, this study]**
	4	*8*	*15*	*10*	**38**	**19**	**45.5**	**EPMA; [LMV this study]**
GOR132-G*	22	2	1.8	0.2	6.2	1	45.5	SIMS; [1]
			50	50	30	30		EPMA; [1]
					50	75		EPMA; [1]
	<d.l.		5.7	0.2	30	0.6		SIMS; [WHOI this study]
	<d.l.		**5.8**	**0.3**	**27**	**1.0**		**SIMS; [eq. 6, this study]**
	4	*8*	*11*	*13*	**24**	**17**	**44.3**	**EPMA; [LMV this study]**
VG2*, *aka* USNM 111240/52	334	14					50.6	SIMS; [4]
			1348	124	291	104		EPMA; [5]
			1365	58	316	38		EPMA; [5]
			1340	160				EPMA; [6]
			1305	135				EPMA; [7]
			1200	160	270	80		EPMA; [8]

			1416	72	303	112		EPMA; [9]
			1500					EPMA; [10]
	243	36	1441	55	325	15		SIMS; [WHOI this study]
	223	**26**	**1352**	**66**	**249**	**28**		**SIMS; [eq. 6, this study]**
	210	*66*	**1343**	**23**	**306**	**13**		**EPMA; [LMV this study]**
VG-A99*, aka A99, USNM 113498/1			170	60				EPMA; [6]
			135	100	229	80		EPMA; [5]
	765	158	220	48	227	40		EPMA; [5]
			177	42	212	62		EPMA; [9]
			96	63				EPMA; [7]
			200	100				EPMA; [11]
	709	47					51.1	SIMS; [4]
	976	8						EPMA; [12]
			175	116	205	60		EPMA; [13]
	799	104	141	5	220	10		SIMS; [WHOI this study]
	734	**76**	**132**	**6**	**170**	**18**		**SIMS; [eq. 6, this study]**
	597	**49**	**130**	**11**	**210**	**10**		**EPMA; [LMV this study]**
Sletta	**3306**	**340**	**28**	**18**	**2075**	**64**		**EPMA; [LMV this study]**
KL2-G*	177	28	7.7	1.3	22.4	4.5	50.3	SIMS; [1]
			90	54	40	32		EPMA; [1]
			320	320	60	18		EPMA; [1]
	114;101;128	2;2;4						EPMA, SIMS, PIGE; [2]
	114	20	9.1	0.3	45	1		SIMS; [WHOI this study]
	104	**14**	**8.9**	**0.3**	**38**	**2**		**SIMS; [eq. 6, this study]**
	99	*154*	*23*	*15*	**51**	**23**	**50.5**	**EPMA; [LMV this study]**
	<71				**<324**			**ERDA; [Zurich this study]**
ATHO-G*	770				530		74.5	EPMA; [14]
	0.7	0.07	0.6	0.07	2430	0	75.6	SIMS; [1]
			50	50	570	114		EPMA; [1]
			200	140	510	102		EPMA; [1]
	900	900	240	240	400	160		EPMA; [1]
	1464	186	4.8	0.2	681	32		SIMS; [WHOI this study]
	637	**137**	**4.4**	**0.4**	**512**	**60**		**SIMS; [eq. 6, this study]**
	668	**204**	*17*	*12*	**453**	**22**	**74.1**	**EPMA; [LMV this study]**
	637	**158**			**334**	**196**		**ERDA; [Zurich this study]**
KE12*	4338	1096						EPMA; [15]
	4400							EPMA; [15]
					3270	110	70.8	EPMA; [16]
	4200				3300			EPMA; [16]
	4000	240						Selective ion method; [17]
					3225	160		EPMA; [18]
					3200	800		EPMA; [19]
	4513	88						EPMA; [12]
	7537	932	290	11	4668	226		SIMS; [WHOI this study]
	3898	**689**	**208**	**13**	**3483**	**423**		**SIMS; [eq. 6, this study]**
	4488	**151**	**150**	**14**	**3414**	**55**		**EPMA; [LMV this study]**

	3848	**230**			**3483**	**400**		**ERDA; [Zurich this study]**
Alvin 2390-5	630	44			241	19		SIMS; [20]
	303	**35**	**1270**	**9**	**358**	**5**	**49**	**EPMA; [LMV this study]**
Alvin 2746-15	**123**	**2**	**1449**	**15**	**890**	**9**	**50**	**EPMA; [LMV this study]**

[1] Jochum et al. 2006; [2] Guggino and Hervig, 2010; [3] Diaz et al. 2006; [4] Straub & Layne 2003; [5] Thordasson et al. 1996; [6] Dixon et al. 1991; [7] Thornber et al., 2002; [8] Coombs et al. 2004; [9] DeHoog et al. 2001; [10] Hall et al. 2006; [11] Fisk & Kelley 2002; [12] Witter & Kuehner, 2004; [13] Streck & Wacaster 2006; [14] Oskarsson et al. 1982; [15] Palais and Sigurdsson, 1989; [16] Métrich & Rutherford, 1991; [17] Mosbah et al, 1991; [18] Marianelli et al. 1995; [19] Cioni et al. 1998. [20] Le Roux et al., 2006. <d.l. means below detection limit. Numbers in italic are considered below detection limit.

Table 3: Result of error weighted regression of Eq. 5, and Eq. 6

	ak/dk	±	bk/ck	±	Intercept*	±	RRM**
F (Eq. 5)	682	27	-5.0	0.5	-47	38	0.05
F (Eq. 6)	17.8	0.8	-0.185	0.002	-47	38	0.04
S (Eq. 5)	400	11	4.46	0.03	3.3	20	0.42
S (Eq. 6)	19.8	0.6	-0.1466	0.0001	3.3	20	0.23
Cl (Eq. 5)	14.0	13.6	12.1	0.2	19	17	0.49
Cl (Eq. 6)	12.7	1.5	-0.0057	0.0005	19	17	0.47

* Intercept values are taken from the working curves of Fig. 2. This choice was to reduce cases of erroneous fit coefficients. **RRMS : Reduced residual mean-square value, in which residual of fit values were normalized by the uncertainty of the standards, and the mean value of the sum of the square is reported. When RRMS > 1 indicates that fitted values on average plot outside of 1 sigma of the standard value.

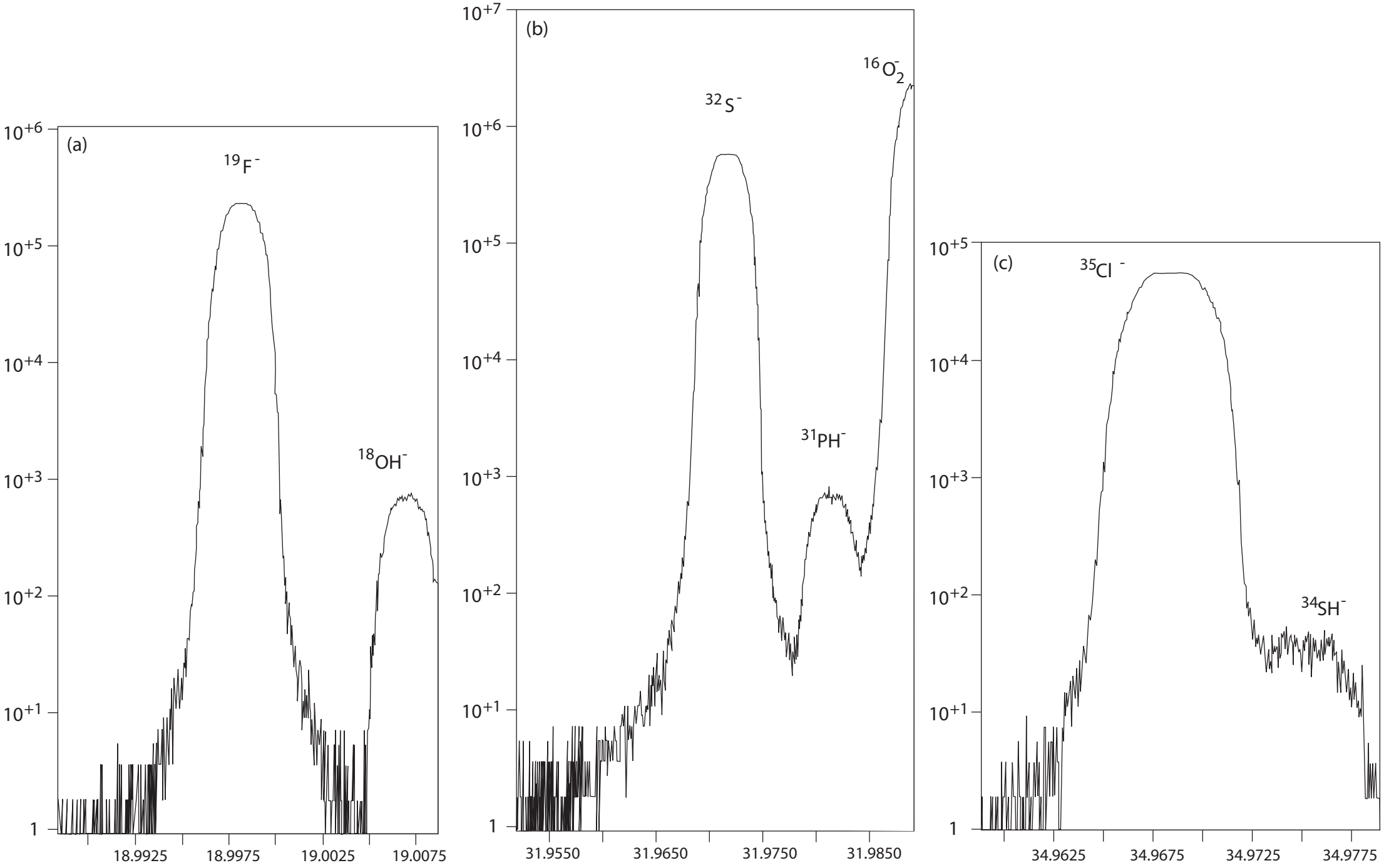
(a)
$^{19}F^-$
$^{18}OH^-$
10^{+6}
10^{+5}
10^{+4}
10^{+3}
10^{+2}
10^{+1}
1
18.9925
18.9975
19.0025
19.0075
(b)
$^{16}O_2^-$
$^{32}S^-$
$^{31}PH^-$
10^{+7}
10^{+6}
10^{+5}
10^{+4}
10^{+3}
10^{+2}
10^{+1}
1
31.9550
31.9650
31.9750
31.9850
(c)
$^{35}Cl^-$
$^{34}SH^-$
10^{+5}
10^{+4}
10^{+3}
10^{+2}
10^{+1}
1
34.9625
34.9675
34.9725
34.9775

Fig. 1

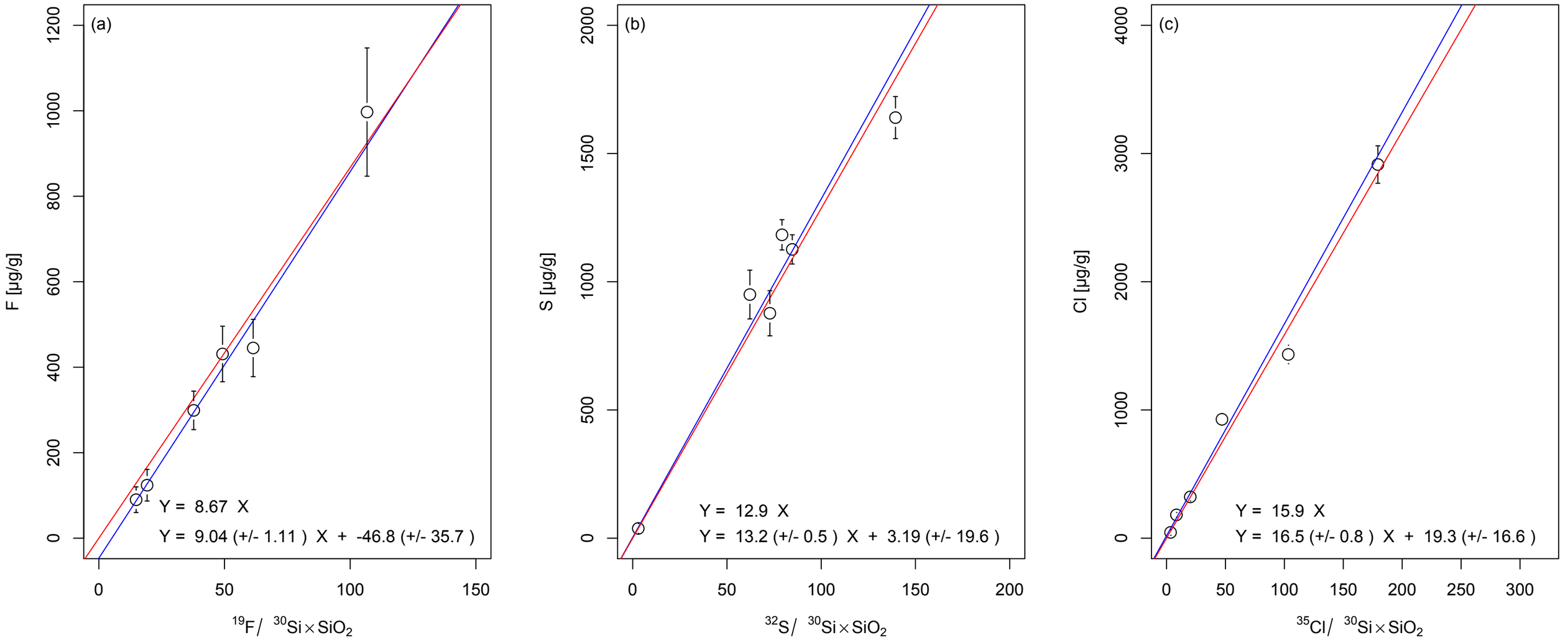
(a)
F [µg/g]
0
200
400
600
800
1000
1200
0
50
100
150
$^{19}F/\ ^{30}Si \times SiO_2$
Y = 8.67 X
Y = 9.04 (+/- 1.11) X + -46.8 (+/- 35.7)
(b)
S [µg/g]
0
500
1000
1500
2000
0
50
100
150
200
$^{32}S/\ ^{30}Si \times SiO_2$
Y = 12.9 X
Y = 13.2 (+/- 0.5) X + 3.19 (+/- 19.6)
(c)
Cl [µg/g]
0
1000
2000
3000
4000
0
50
100
150
200
250
300
$^{35}Cl/\ ^{30}Si \times SiO_2$
Y = 15.9 X
Y = 16.5 (+/- 0.8) X + 19.3 (+/- 16.6)

Fig. 2

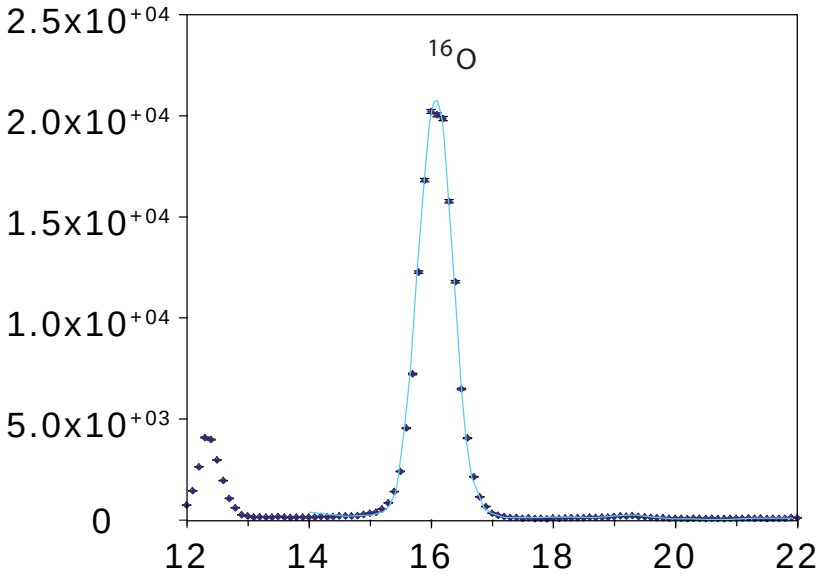
2.5x10+04
2.0x10+04
1.5x10+04
1.0x10+04
5.0x10+03
0
16O
12
14
16
18
20
22

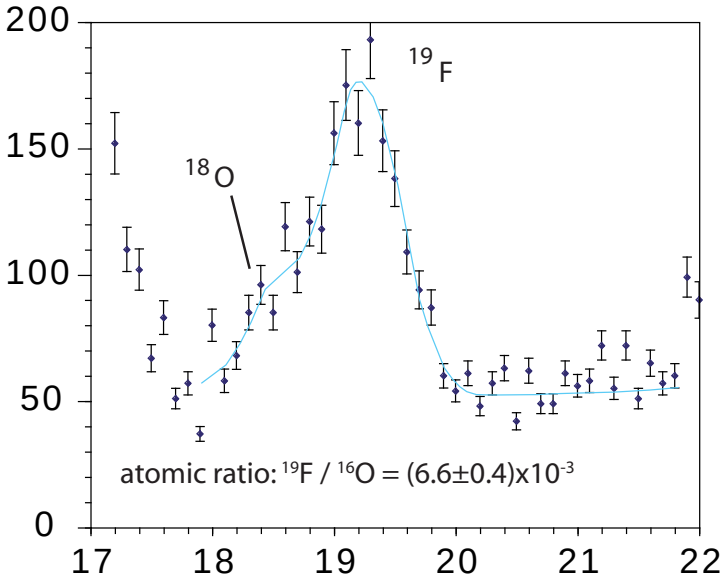
200
150
100
50
0
19F
18O
atomic ratio: 19F / 16O = (6.6±0.4)x10-3
17
18
19
20
21
22

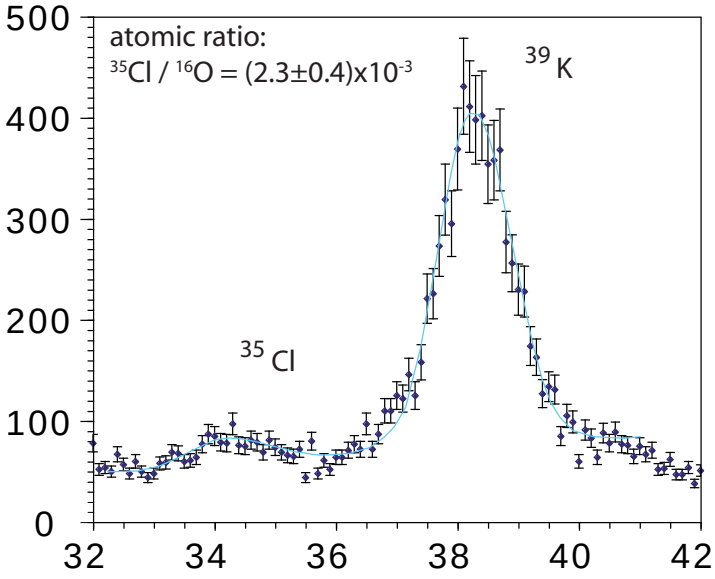
500
400
300
200
100
0
atomic ratio:
35Cl / 16O = (2.3±0.4)x10-3
39K
35Cl
32
34
36
38
40
42

Fig. 3

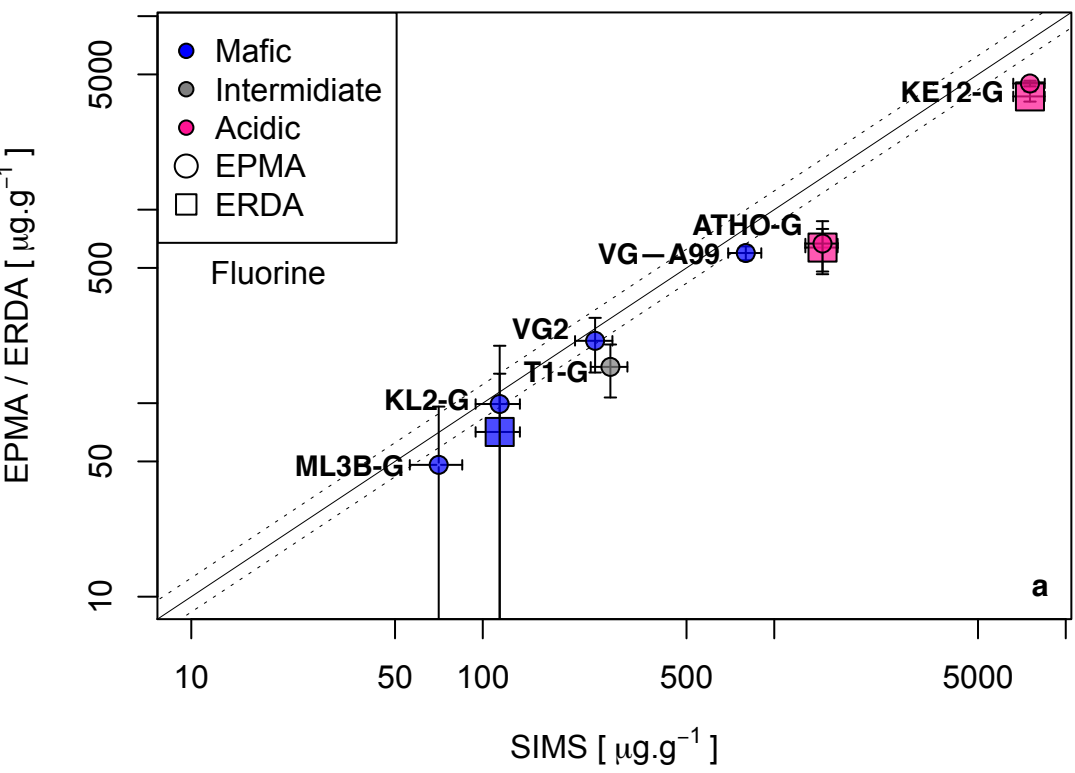
Mafic
Intermidiate
Acidic
EPMA
ERDA
Fluorine
KE12-G
ATHO-G
VG—A99
VG2
T1-G
KL2-G
ML3B-G
a
EPMA / ERDA [μg.g⁻¹]
SIMS [μg.g⁻¹]
10
50
100
500
5000

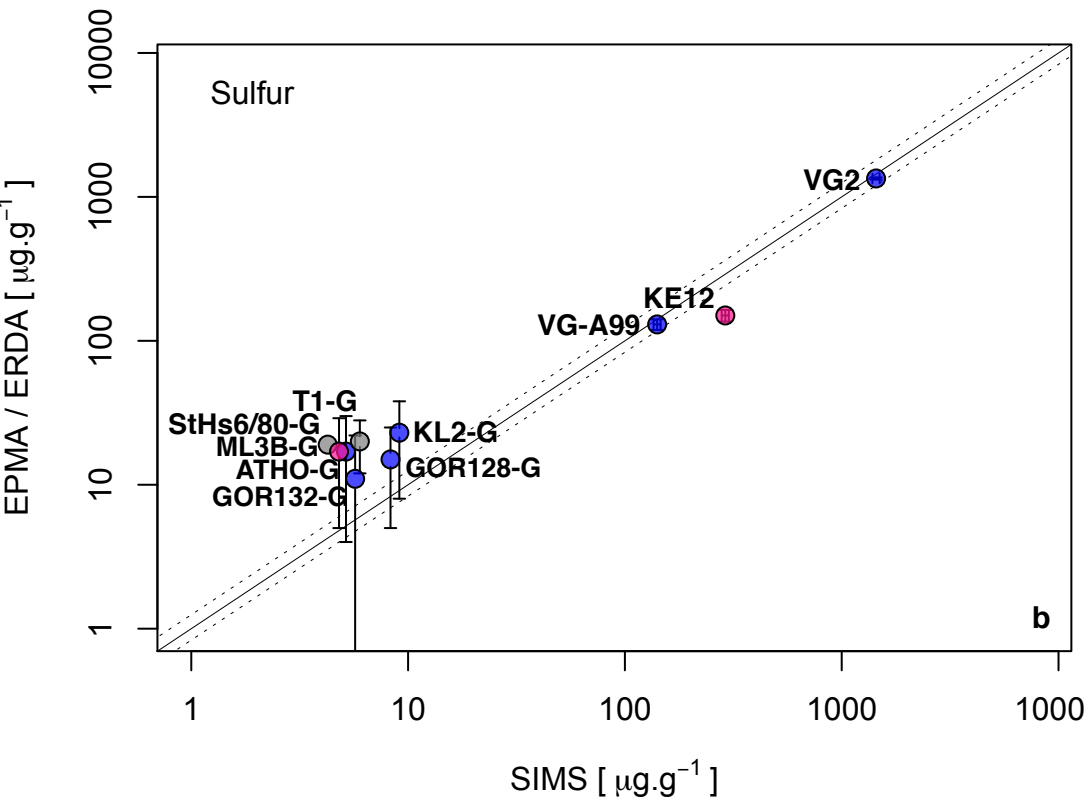
Sulfur
VG2
KE12
VG-A99
T1-G
StHs6/80-G
ML3B-G
ATHO-G
GOR132-G
KL2-G
GOR128-G
b
EPMA / ERDA [μg.g⁻¹]
SIMS [μg.g⁻¹]
1
10
100
1000
10000

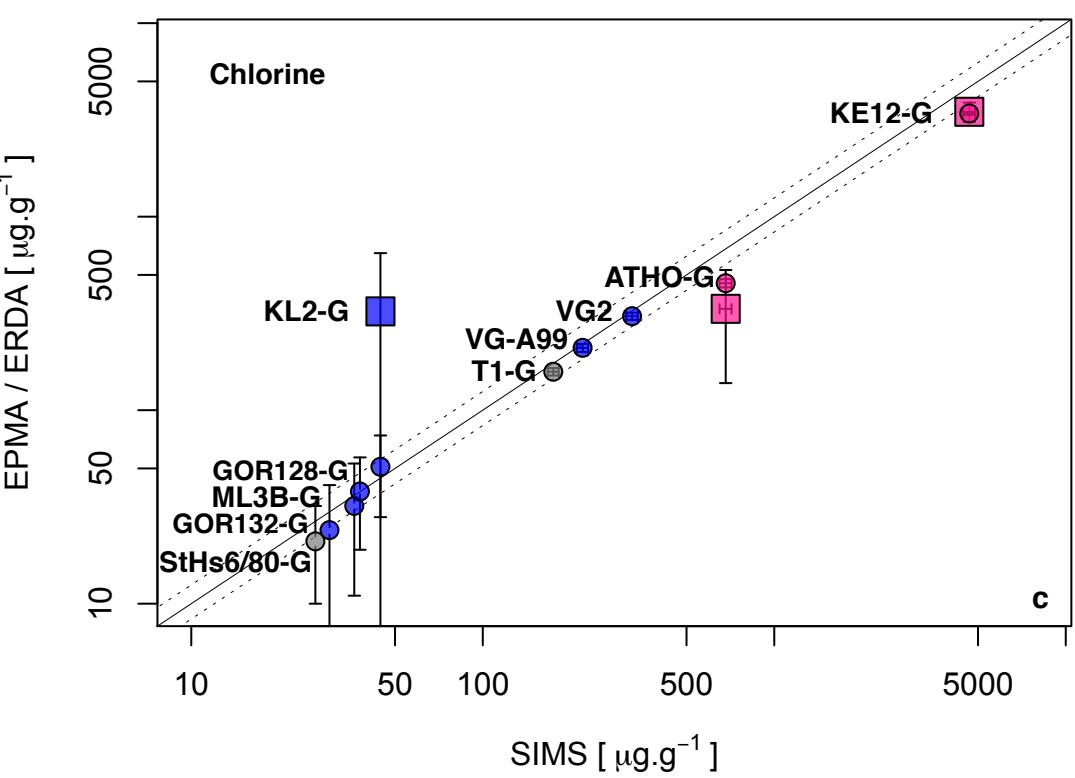
Chlorine
KE12-G
ATHO-G
KL2-G
VG2
VG-A99
T1-G
GOR128-G
ML3B-G
GOR132-G
StHs6/80-G
c
EPMA / ERDA [μg.g⁻¹]
SIMS [μg.g⁻¹]
10
50
100
500
5000

Fig. 4

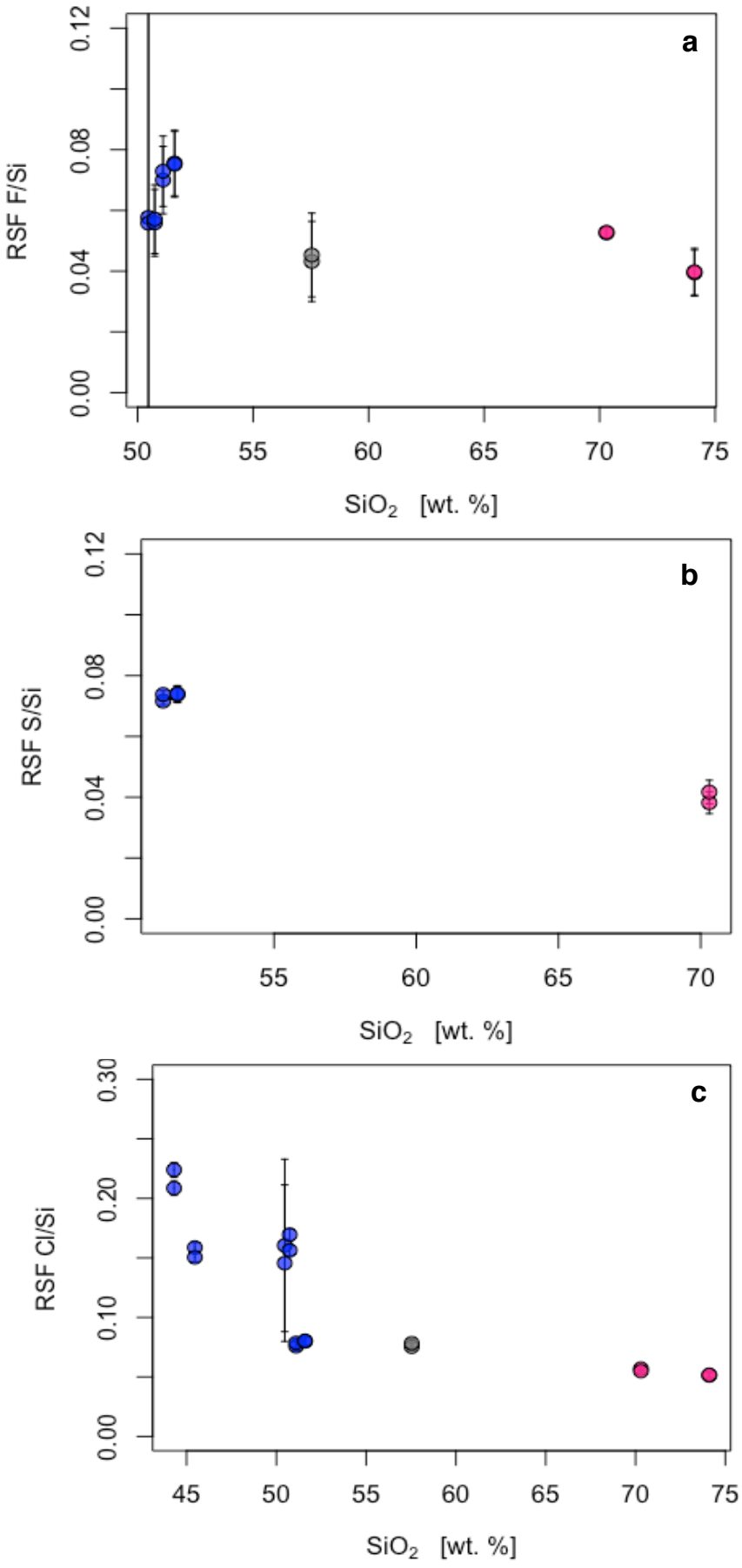
a
RSF F/Si
0.00
0.04
0.08
0.12
50
55
60
65
70
75
SiO2 [wt. %]
b
RSF S/Si
0.00
0.04
0.08
0.12
55
60
65
70
SiO2 [wt. %]
c
RSF Cl/Si
0.00
0.10
0.20
0.30
45
50
55
60
65
70
75
SiO2 [wt. %]

Fig. 5

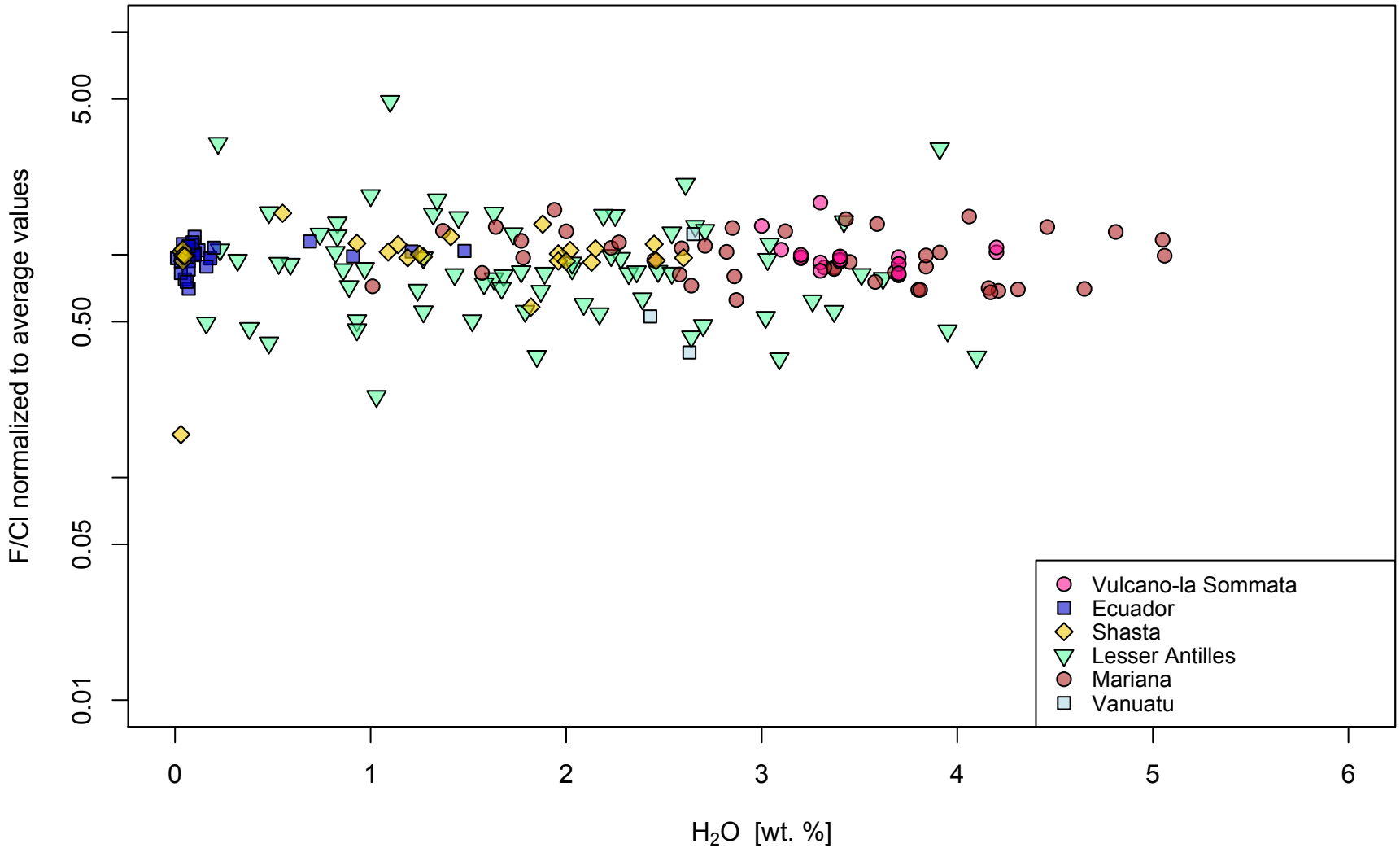
F/Cl normalized to average values
0.01
0.05
0.50
5.00
0
1
2
3
4
5
6
H2O [wt. %]
Vulcano-la Sommata
Ecuador
Shasta
Lesser Antilles
Mariana
Vanuatu

Fig. 6